Available online at www.sciencedirect.com

ScienceDirect

Ceramics International 41 (2015) 11279–11286

CERAMICS INTERNATIONAL

www.elsevier.com/locate/ceramint

Multicolored photoluminescence and structural properties of zirconium oxide films co-doped with Tb^{3+} and Eu^{3+} ions

A.I. Ramos-Guerra[a], J. Guzmán-Mendoza[a], M. García-Hipólito[b,*], O. Alvarez-Fregoso[b], C. Falcony[c]

[a]*Centro de Investigación en Ciencia Aplicada y Tecnología Avanzada del Instituto Politécnico Nacional, Legaría 694 Colonia Irrigación, Mexico D.F. C.P. 11500, Mexico*

[b]*Instituto de Investigaciones en Materiales, Universidad Nacional Autónoma de México, Apdo. Postal 70-360, Delegación Coyoacán, Mexico D.F. C.P. 04150, Mexico*

[c]*Departamento de Física, Centro de Investigación y de Estudios Avanzados del Instituto Politécnico Nacional, Apdo. Postal 14-470, Delegación Gustavo A. Madero, Mexico D.F. C.P. 07000, Mexico*

Received 28 March 2015; received in revised form 14 May 2015; accepted 16 May 2015
Available online 22 May 2015

Abstract

The photoluminescence and structural properties of ZrO_2 films doped with Eu^{3+} and Tb^{3+} ions, deposited by ultrasonic spray pyrolysis technique, are reported. X ray diffraction analysis showed that the films are polycrystalline and exhibit the ZrO_2 tetragonal metastable phase. The surface morphology characteristics of the films are strongly dependent on the deposition temperature, going from a rough surface formed by ramifications at low temperatures to a denser material with ramifications and the appearance of spherical features at higher temperatures. In addition, the elemental composition of the films as determined by energy dispersive spectroscopy, is reported. The photoluminescence spectra present the characteristic emission peaks associated with the Tb^{3+} and Eu^{3+} dopants as well as a broad emission peaked at 440 nm associated with radiative transitions within the ZrO_2 matrix. As the deposition temperature is increased, it was observed an increasing intensity of the photoluminescence emission. Also a concentration quenching was observed for both dopants. The photoluminescence emission spectra for the ZrO_2 films co-doped with Eu^{3+} and Tb^{3+} ions, showed emission lines that are a combination of those observed for each ion individually plus the blue broad band associated with the host lattice. Decay times were measured for double doped samples. The CIE chromaticity diagrams for these films showed colors falling in the blue, green, yellow, red-orange, bluish-white and yellowish-white regions depending on the doping characteristics of the films.

Keywords: A. Films; Tb^{3+}; Multicolored luminescence; ZrO_2:Eu^{3+}; Spray pyrolysis

1. Introduction

Luminescent materials play an important role in the development of new applications such as different types of flat panels and projection displays and white light lamps. The performance of display panels is strongly related to the nature of the phosphor, to its chemical and physical stability and the kind of optical centers active in them. There are several types of flat luminescent display technologies under development, among them are: plasma display panels (PDP), in which three primary color phosphors are excited by vacuum ultraviolet (VUV) radiation generated by a plasma; field emission displays (FED), in which the luminescent material is irradiated by low-energy electrons; and thin film electroluminescence displays (ELD), in which electrons injected into the luminescent layer are accelerated by an applied field up to the energy necessary to excite luminescent centers [1–3]. On the other hand, white light sources of high-efficiency, high brightness and low energy consumption are required for outdoor illumination and full-color display applications. During the last 10 years white LEDs have become very important lighting sources and the development of phosphors for white LEDs and colored light generation must be considered an important

*Corresponding author. Tel.: +52 5556224598; fax: +52 5556161371.
E-mail address: maga@unam.mx (M. García-Hipólito).

http://dx.doi.org/10.1016/j.ceramint.2015.05.084
0272-8842/

market driver in the future [4–5]. Metal oxides are very versatile materials that may play an important role in the phosphors design and synthesis technology. Among them, zirconium oxide is a material whose properties make it an excellent candidate for applications in the field of the optics in general, due to its high refraction index (~2.17) and high transparency for visible-ultraviolet light. In the case of luminescent applications, the ZrO_2 has shown to be a good host for a great variety of rare earth ions [6–8] because of its wide band gap of about 5.2–5.8 eV and their low phonon frequency of about 470 cm^{-1}, which increases the probability of occurrence of radiative transitions when this material is doped with rare earths or transition metals. There are some studies on ZrO_2 and HfO_2 powders optically activated with $Eu^{3+}+Tb^{3+}$ ions [9,10] but, to our best knowledge, research on films of ZrO_2: $Eu^{3+}+Tb^{3+}$ is scarce or nonexistent. Luminescent films, as compared with materials in powder form, have some advantages such as good adhesion to the substrate, unaltered properties throughout the covered area, better thermal stability, and minimal optical scattering with less material [11]. More than one method has been used to synthesize ZrO_2 films [12,13], among them are: sol–gel, atomic layer deposition, solid state reaction and spray pyrolysis [14–16]. The ultrasonic spray pyrolysis has been successfully used to deposit different metal oxide films [17,18]. This is a low cost technique with high deposition rates, easy to operate and with the capability to carry out depositions on large areas.

This work reports the photoluminescence characteristics of zirconium oxide films co-doped with different concentrations of Eu^{3+} and Tb^{3+} ions, with the purpose of achieving light photoemission of various colors (including white light) by tuning the concentrations of the dopants and selecting the excitation wavelength. In addition, the surface morphology, the chemical composition and the crystalline structure of the films were analysed as a function of the deposition parameters.

2. Materials and methods

The un-doped films were deposited using $ZrCl_2 \cdot 8H_2O$ (99.99% Aldrich), dissolved in deionized water, the solution molarity was 0.6M. The films were deposited on corning glass, at deposition temperatures (T_s) from 350 °C to 600 °C, in steps of 50 °C; using filtered air as carrier gas at a rate of 10 l/min. The ultrasonic frequency was 1.6 MHz. The deposition time was adjusted in the range of 5–6 min in order to obtain a thickness of approximately 5 μm, as measured by a Sloan Dektak IIA profilometer, for all samples. The Tb and Eu concentrations were varied from 0 to 15 at% (atomic percent), measured with respect to the zirconium content. The rare earth precursor salts were $EuCl_3 \cdot 6H_2O$ (99.99%) and $TbCl_3 \cdot 6H_2O$ (99.99%), both from the Aldrich Chemical Co. The best emission intensity for Eu and Tb were 5 at% and 10 at%, respectively. Taking in consideration these results, co-doped films were deposited using a combination of the spraying solutions used for ZrO_2: Eu^{3+} (5 at%) and ZrO_2:Tb^{3+} (10 at %); the mechanism was to keep a constant volume of 100 ml changing the content of each of these solutions from 0, 20, 40, 50, 60, 80 and 100 ml, thus, seven solutions, labeled as D0 to D6 were prepared (see Table 1). All samples were analysed by XRD with a Siemens Diffractometer model D-5000, using the $K\alpha$ wavelength of the copper ($\lambda = 1.542$ Å). A step of 0.05° between 20° and 70° with scan of 0.5 s for each step was used. The surface morphology study was carried out with a JEOL-6390LV scanning electron microscopy (SEM), operating at 20 kV, using the secondary electron signal. The determination of the chemical elements present in the samples was done by energy dispersive spectroscopy (EDS), using an Oxford INCA X-sight, silicon–lithium (Si–Li) X-ray detector, installed in the above-mentioned electron microscope. The photoluminescence (PL) and decay time measurements were performed at ambient temperature using a FluoroMax-P Jobin Yvon Horiba spectrofluorimeter, with a Xenon excitation source of 150 watts of continuous and pulsed emission.

3. Results and discussion

Fig. 1 shows the indexed X-ray diffraction patterns, for the ZrO_2 un-doped films as a function of the deposition temperature. It can be observed that all the films have certain degree of crystallinity; even those deposited at low temperatures; the diffractograms show wide peaks with relatively low intensity, which can mean that the films are formed by very small crystals or a combination of these with an amorphous phase. The films deposited at 450, 500, 550 °C and 600 ºC, show

Table 1
Combinations of the precursor solutions for the deposition of the ZrO_2: $Tb^{3+}+Eu^{3+}$ films.

Deposition solutions
D0 = 100 ml (ZrO_2:5%Eu^{3+})
D1 = 80 ml (ZrO_2:5%Eu^{3+}) + 20 ml (ZrO_2:10%Tb^{3+})
D2 = 60 ml (ZrO_2:5%Eu^{3+}) + 40 ml (ZrO_2:10%Tb^{3+})
D3 = 50 ml (ZrO_2:5%Eu^{3+}) + 50 ml (ZrO_2:10%Tb^{3+})
D4 = 40 ml (ZrO_2:5%Eu^{3+}) + 60 ml (ZrO_2:10%Tb^{3+})
D5 = 20 ml (ZrO_2:5%Eu^{3+}) + 80 ml (ZrO_2:10%Tb^{3+})
D6 = 100 ml (ZrO_2:10%Tb^{3+})

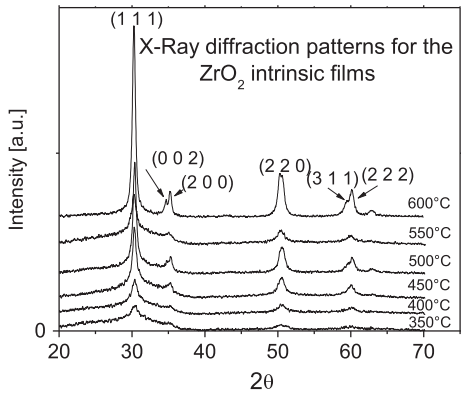

Fig. 1. XRD patterns for ZrO_2 films grown at different T_s: 350 °C, 400 °C, 450 °C, 500 °C, 550 °C and 600 °C.

better defined peaks; a narrow and high peak centered at $2\theta = 32.0^\circ$ and wide peaks centered at 35.0°, 50.0° and 60.0° can be observed. Even when the width of the peaks in the diffraction patterns is related to a small size of crystal, in this case, the widening that appears with the increase of the deposition temperature in the peaks of diffraction centered at 35.0°, 50.0° and 60.0° may be related to the nano-structured character of the material as well with the doublets and triplets of the tetragonal phase of the zirconium oxide. According with Scherrer's equation, the crystal size is around 17 nm, for the sample deposited at 550 °C. Sometimes the tetragonal phase is reported as a cubic phase, since some peaks correspond to the characteristic reflections of this phase; however, the peaks apparently belonging to the cubic phase, are not anything else than the characteristic doublets of the tetragonal phase, masked by the widening of the diffraction lines due to the nanos-tructured character of the material. The occurrence of the ZrO_2 metastable tetragonal phase may be related to the intrinsic properties of the film namely, small average crystallite size, large specific surface and appreciable excess energy [19]. Finally, the diffractogram of the film deposited at 600 °C presents intense well defined peaks, which indicates the improvement in the crystalline quality of the material.

Fig. 2 shows the SEM micrographs for the un-doped ZrO_2 films deposited at 350, 400, 550 and 600 °C. All films present a rough surface, whose morphology depends on the substrate temperature during the deposition. At low temperatures (Fig. 2a), the films show a continuous and rough surface formed by ramifications, hollows or caverns and some spherical particles. At these low deposition temperatures, we can assume that the aerosol reach the substrate in liquid phase, allowing to generate a process known as coagulation, in which two or more drops collide and may join to form a bigger drop. A more careful analysis allows visualizing that these ramifications present wider zones, which match in size with the diameter of the spherical aerosol drops and could indicate that these ramifications are the result of the union of many drops in the coagulation process, which will be present as long as there is a liquid or semi-liquid phase. With the increase of the deposition temperature (Fig. 2b), the films do not show clear areas of the substrate, however, the roughness of the surface increases, appearing a surface morphology also with branched forms and a large amount of spherical particles. Experimentally it has been found that the coagulation time is relatively un-affected by the temperature, but depends strongly on the density of the drops of the precursor material, whereas bigger the density of the drops, the faster the coagulation. So, if the concentration of the precursors is high, these can propitiate a greater coagulation. These high concentrations can also propitiate the appearing of a greater amount of spherical particles with the increment of the substrate temperature. Therefore presence of these spherical particles can be attributed to the high solubility of the precursor elements in water, giving place to a great difference between the critical super-saturation and the equilibrium saturation, making these precursors elements more susceptible to produce solid particles, since, solutes with a higher degree of super-saturation tend to form a great number of crystals, maybe with a size around nanometers, generating particles with spherical shape [20]. For higher deposition temperatures (550 °C, Fig. 2c), the films still

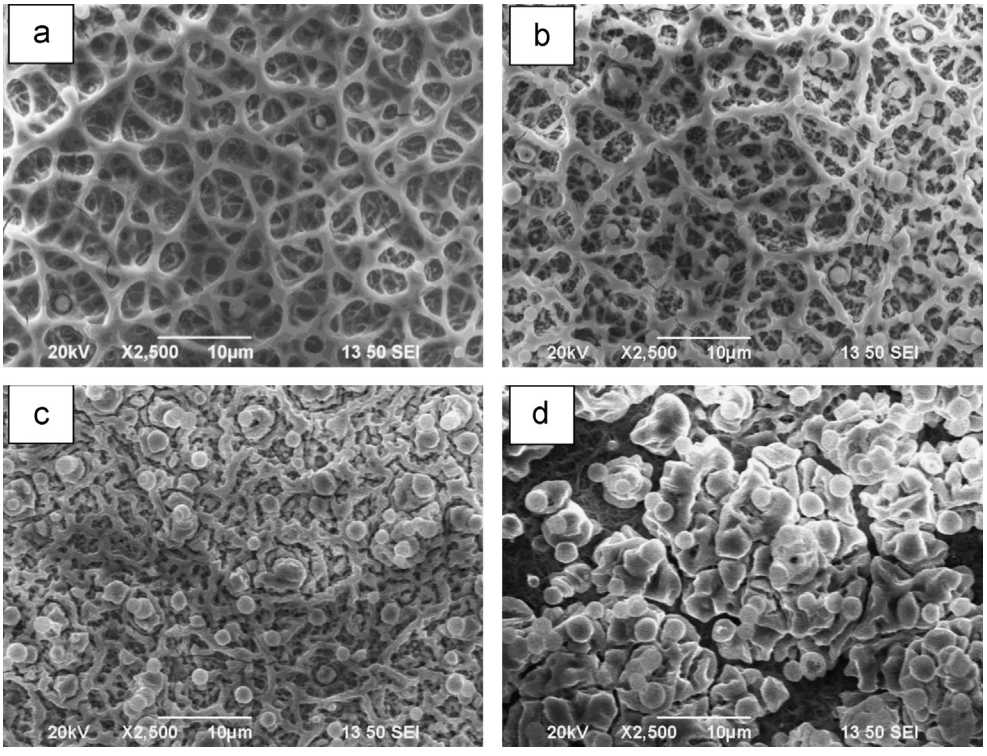

Fig. 2. SEM micrographs from surface morphology of ZrO_2 films as a function of the T_s: (a) 350 °C, (b) 400 °C, (c) 550 °C and (d) 600 °C.

appears adhered to the substrate with a more dense surface. Also, the films have a larger amount of spherical particles. This structure with more closed ramifications could be related with the presence of less amount of the liquid phase and a greater amount of the vapor phase, giving place to a greater incorporation of spherical particles. Finally, for the highest deposition temperature (600 ºC, Fig. 2d), the films show agglutination of the material on the upper layers, which, were deposited on the vestiges of the first layers that are formed by ramifications and smaller spheres, generating discontinuities on their surface. This surface morphology can be associated to the fact that at higher deposition temperatures, the precursor elements may react before they reach the substrate, generating a very fine powder of the metallic oxide, which is, what conforms the upper layer of the film. The observed discontinuities on the film may be due to increment of the mechanical stress on the surface of the substrate produced by the increment of the substrate temperature. Films deposited at 550 °C showed the best mechanical characteristics with fewer discontinuities and with good adherence to the substrate; thus, these films deposition conditions were chosen for the later characterization.

Fig. 3 shows the EDS measurements for Tb, Eu and Cl for ZrO_2: $Eu^{3+}+Tb^{3+}$ films as a function of the different combinations of the spraying solutions prepared, as described above (see Table 1), from solutions with different amounts of Eu^{3+} (5 at%) and Tb^{3+} (10 at%) deposited at 550 °C. It can be observed that the amount of terbium and europium, behaves in agreement with the expected, due to the proportion of these elements in the precursor solution, i.e., as the amount of terbium increases in the films, the amount of europium decreases and vice versa. On the other hand, it is interesting to notice that for the sample labeled as D2, the amount of each rare earth is almost the same. Despite not being in the figure, the amount of zirconium and oxygen within the samples was also recorded, including the samples labeled as D0, D6 and an un-doped sample; obtaining an amount of oxygen which remains almost constant, with an average value of 68.24 at%; close to the ideal value of 66 at% in the ideal ZrO_2. In the case of zirconium (Zr), this remains practically constant with an average value of 25.98 at%. However, this value is relatively far from the ideal value of 33 at%, which may be due the incorporation of Cl; since, all the films show an important amount of chlorine. It is convenient to mention that in EDS measurements on films with a single impurity (Eu or Tb); in all the cases a decrease in the amount of chlorine was observed with the increment of the deposition temperature. This result may be due the fact that at higher temperatures, a greater dissociation and evaporation of the precursor components is promoted. Besides, with the increment of the substrate temperature, there is a greater superficial thermal energy, propitiating a better crystallization of the films, reducing the incorporation of the chlorine as compared with lower substrate temperatures. In general, it can be seen that at the deposition temperature of 550 °C, there is a better incorporation of the Tb^{3+} ions, which could be explained considering the atomic radios of these two elements, since the terbium ion has an atomic radio closer to zirconium, which allows a better incorporation inside the host crystalline structure.

PL emission measurements were performed on ZrO_2, ZrO_2: Eu^{3+}, ZrO_2: Tb^{3+} and ZrO_2: $Eu^{3+}+Tb^{3+}$ films. For the single doped films, the results obtained are in agreement with previous reports [21], reaching the best luminescent emission with 5 at% (Eu) and 10 at% (Tb); a concentration quenching is observed for higher doping concentration in both cases.

Fig. 4 shows the excitation spectra for ZrO_2, ZrO_2: Eu^{3+} (5 at%), ZrO_2: Tb^{3+} (10 at%) films (all deposited at 550 °C). These spectra were recorded fixing the emission wavelengths at 420, 607 and 544 nm, respectively. In the case of ZrO_2: Eu^{3+} (5 at%), D0 sample, this spectrum shows a wide band corresponding to a charge transfer band (CTB) centered at 258 nm, which is originated from electron transitions from 2p orbitals of O^{-2} ions to 4f orbitals of the Eu ions. In addition, it is possible to observe bands with minor intensities which correspond to characteristic 4f–4f absorptions of the Eu^{3+} ions. In the case of the ZrO_2: Tb^{3+} (10 at%) film, sample D6, the charge transfer band is centered at 288 nm. Also, it is possible to observe bands with minor intensities which correspond to typical 4f–4f absorptions of the Tb^{3+} ions.

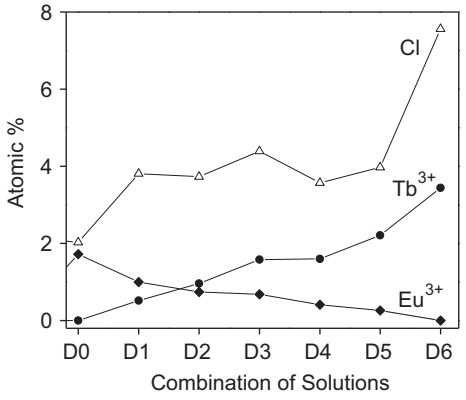

Fig. 3. Atomic percent content of chlorine, terbium and europium into ZrO_2: Eu^{3+} (5 at%)+Tb^{3+} (10 at%) films with different combinations. The films were deposited at 550 °C.

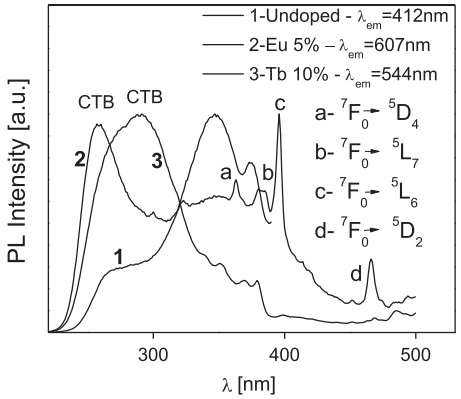

Fig. 4. PL excitation spectra for ZrO_2, ZrO_2: Eu (5%) and ZrO_2:Tb(10%) films deposited at 550 °C. The emission wavelengths were fixed at 420, 607 and 544 nm, respectively.

The un-doped sample presents a broad band peaked at 348 nm associated to defects of the ZrO_2 lattice.

Fig. 5 shows the PL emission spectra for ZrO_2, ZrO_2: Eu^{3+} (5 at%), ZrO_2: Tb^{3+} (10 at%) films (all deposited at 550 ºC), these spectra were recorded exciting with 348, 258 and 288 nm, respectively (these values were obtained from Fig. 4). The spectrum for ZrO_2: Eu^{3+} (5 at%) show weak peaks for the forbidden transitions at 578 and 653 nm and peaks with higher intensity at 591 ad 607 nm. It has been reported [22] that when the transition at 607 nm is higher than that at 591 nm, the europium occupies sites of lower symmetry without inversion centers into the crystalline structure; the emission peaks are quite wide, which suggest the europium ions are located in less ordered and low symmetry surroundings [23]. Also, it is observed, the PL emission spectrum for the ZrO_2:Tb^{3+} (10 at%) films, which shows the characteristic bands of the electronic transitions of trivalent terbium, with the strongest emission located at 544 nm; it can be observed a splitting of this peak, which is the result of the spin–orbit interaction under the crystalline field surrounding the dopant. It is important to mention, that the PL emission of the host lattice

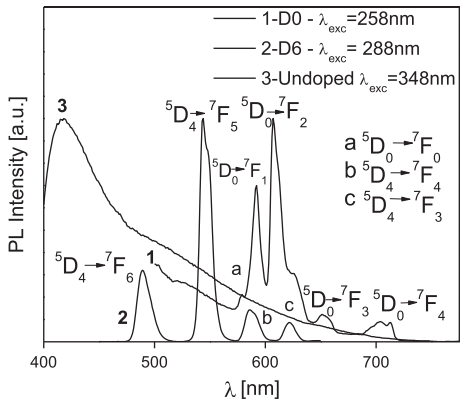

Fig. 5. PL emission spectra for ZrO_2, ZrO_2: Eu^{3+} (5 at%), ZrO_2: Tb^{3+} (10 at %) films deposited at 550 °C. The excitation wavelengths were 348, 258 and 288 nm, respectively.

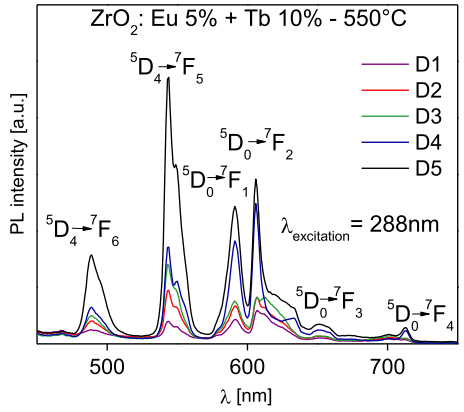

Fig. 6. PL emission spectra for ZrO_2:Tb^{3+} + Eu^{3+} films deposited at 550 °C as a function of the different solution combinations (D1, D2, D3, D4 and D5). The excitation wavelength was 288 nm. (For interpretation of the references to color in this figure legend, the reader is referred to the web version of this article.)

(ZrO_2) exhibits a intense broad band centered at 420 nm within the blue region, this is an important feature, since combining a red (Eu^{3+}), green (Tb^{3+}) and blue (ZrO_2), emissions, it would be possible to reach a film with emission in various colors including white light.

Fig. 6 shows the PL emission spectra ZrO_2: Eu^{3+} (5 at%)+ Tb^{3+} (10 at%) films deposited at 550 °C, considering the different combinations of the precursor solutions (as described above), for an excitation wavelength of 288 nm. The spectra show an intensity behavior in accordance with the different combinations of the emission bands belonging to the typical electronic transitions of the europium and terbium ions. This result could indicate an absence of energy transfer between both dopants. In this case, the blue emission from the host is poor. The highest emission belongs to the film identified as D5, where the highest emission peak is at 544 nm, which is assigned to electric dipole transition $^5D_4 \rightarrow {}^7F_5$ of terbium ion, since 288 nm is the best wavelength to excite the Tb ion. In the film identified as D4, a dominant emission in the transitions $^5D_0 \rightarrow {}^7F_1$ and $^5D_0 \rightarrow {}^7F_2$ corresponding to bands 591 nm (orange) and 607 nm (red) from the europium ions are observed. From this figure it is concluded that the ratio Tb/Eu into the ZrO_2 host lattice determine the best emission intensity (emissions from either Tb or Eu). These samples were also excited by 258 nm (best wavelength to excite the Eu ions) these spectra were similar to those showed in Fig. 6.

In Fig. 7 PL excitation and emission spectra for ZrO_2: Eu^{3+} (5 at%)+Tb^{3+} (10 at%) films (samples deposited from solution D1) are exhibited. The excitation spectra (See inset) were recorded fixing the emissions at 440, 544 and 607 nm. It is possible to note wide excitation bands centered at 368 nm (host lattice), 291 nm (Tb ions) and 291 nm (Eu ions). The excitation spectra for the host lattice (440 nm) and Eu ions (607 nm) coincide at 368 and 380 nm. The PL emission spectra were recorded exciting with these two wavelengths, 368 and 380 nm. Here it was observed a broad band peaked at 440 nm (associated to host lattice) and the characteristic emissions from the Tb and Eu ions. The higher overall emission intensity was reached for the excitation with 368 nm.

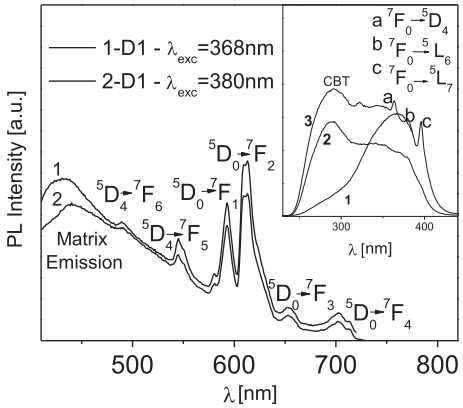

Fig. 7. PL emission and excitation spectra for ZrO_2:Tb^{3+} +Eu^{3+} films (samples deposited from solution labelled as D1) deposited at 550 °C, excited with 368 and 380 nm. The inset shows the excitation spectra fixing the emissions at (1) 440, (2) 544 and (3) 607 nm.

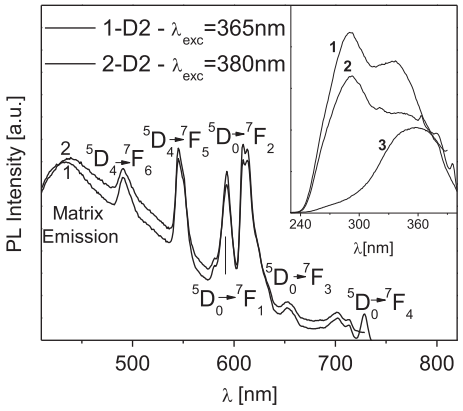

Fig. 8. PL emission and excitation spectra for ZrO_2:Tb^{3+} +Eu^{3+} films (samples deposited from solution labelled as D2) deposited at 550 °C, excited with 368 and 380 nm. The inset shows the excitation spectra fixing the emissions at (1) 440, (2) 544 and (3) 607 nm.

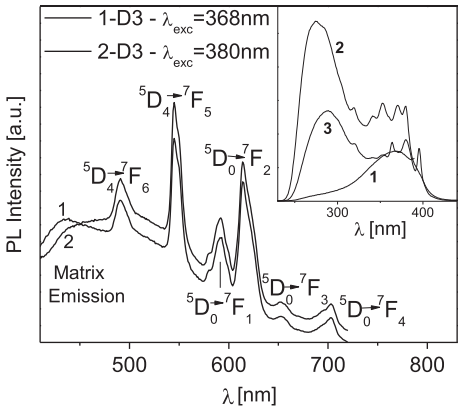

Fig. 9. PL emission and excitation spectra for ZrO_2:Tb^{3+} + Eu^{3+} films (samples deposited from solution labelled as D3) deposited at 550 °C, excited with 368 and 380 nm. The inset shows the excitation spectra fixing the emissions at (1) 440, (2) 544 and (3) 607 nm.

Figs. 8 and 9 show PL excitation and emission spectra for samples deposited from solutions labeled as D2 and D3, respectively. These spectra show very similar characteristics to those exhibited in Fig. 7. Samples deposited from solution D3 exhibited the best emission intensity when excited with 380 nm. The spectra for samples deposited from solutions labeled as D1, D2, and D3 generated colors close to white color. The samples labeled as D4 and D5 produced mainly green emissions when excited in the same conditions for D1, D2 and D3 samples.

The CIE chromaticity diagram (1931) was used to evaluate the performance of the color emission. CIE chromaticity coordinates are obtained from the color matching functions; so any color can be found in terms of its x and y coordinates. In Fig. 10A–D, it can be observed the chromaticity diagrams and the corresponding coordinates (x, y) for the spectra of co-doped ZrO_2 films showed in Figs. 6–9. On each diagram had been indicated the emissions of the samples with different doping concentrations, and excited with two different wavelengths.

Fig. 11 shows the time decay measurements for the peak intensities associated with Tb (544 nm) and Eu (607 nm) of sample D2. Both curves show a behavior that is best fitted, as shown in this figure, with a double exponential decay:

$$I = A_1 e^{(-t/\tau_1)} + A_2 e^{(-t/\tau_2)}$$

where I is the intensity; A_1 and A_2 are constants; t is the time and τ_1 and τ_2 are decay times for exponential components. With these parameters, the average decay times (τ) of rare earth ions were calculated by the following equation:

$$\tau = \frac{A_1\tau_1^2 + A_2\tau_2^2}{A_1\tau_1 + A_2\tau_2}$$

The average decay times calculated from such fit were 1.21 and 0.97 ms. for Tb^{3+} and Eu^{3+} ions, respectively. The decay time for the intrinsic emission from the ZrO_2 host was found to be faster than microsecond response time of our measurement equipment. Further work will be required to properly address this aspect.

Finally, considering the PL emission spectra of doped ZrO_2 films with each of the elements separately and those for the double-doped samples, it is observed that the white emission is due to the contribution of the emission of each ion individually (Eu and Tb) plus the blue emission from the ZrO_2 matrix. It is important to mention that the luminescent emissions from the studied films in this work are seen with naked eye when they are excited with a mercury lamp (366 nm) in the presence of ambient light, which gives an idea of how strong the PL emission intensity is.

4. Conclusions

Un-doped ZrO_2 and single- and double-doped ZrO_2: RE (where RE=Tb^{3+} and Eu^{3+}) films have been synthesized using a simple, economical and versatile ultrasonic spray pyrolysis technique (using short deposition times and relatively low deposition temperatures). The ZrO_2: Tb^{3+} (10 at%): Eu^{3+} (5 at%) films showed white PL as a function of Tb/Eu ratios and the excitation wavelengths. The results thus provide a practical basis for the design of white light illumination sources by blending this kind of phosphor with an appropriate UV emitter; with the development of UV LEDs (340–400 nm), a renewed interest in new phosphors capable of absorbing such a band and emitting in the visible region has been generated. The XRD analysis showed that the ZrO_2 films crystallize in a tetragonal meta-stable crystalline structure for the samples deposited at higher substrate temperature. By the Scherrer formula the estimated size of the constituent crystallites of the studied films was 17 nm. The growth rate of the films was a micrometer per minute. In the surface morphology analysis, it was observed that the samples exhibited rough surfaces; these films showed a branched surface morphology for samples deposited at low substrate temperature which was transformed in a denser material with small clusters of spherical particles when the substrate temperature was increased. On the other hand, the EDS analysis showed an average amount of oxygen of 68.24 at% which is close to the ideal value of 66 at% in the stoichiometric ZrO_2 films. Furthermore the amount of the

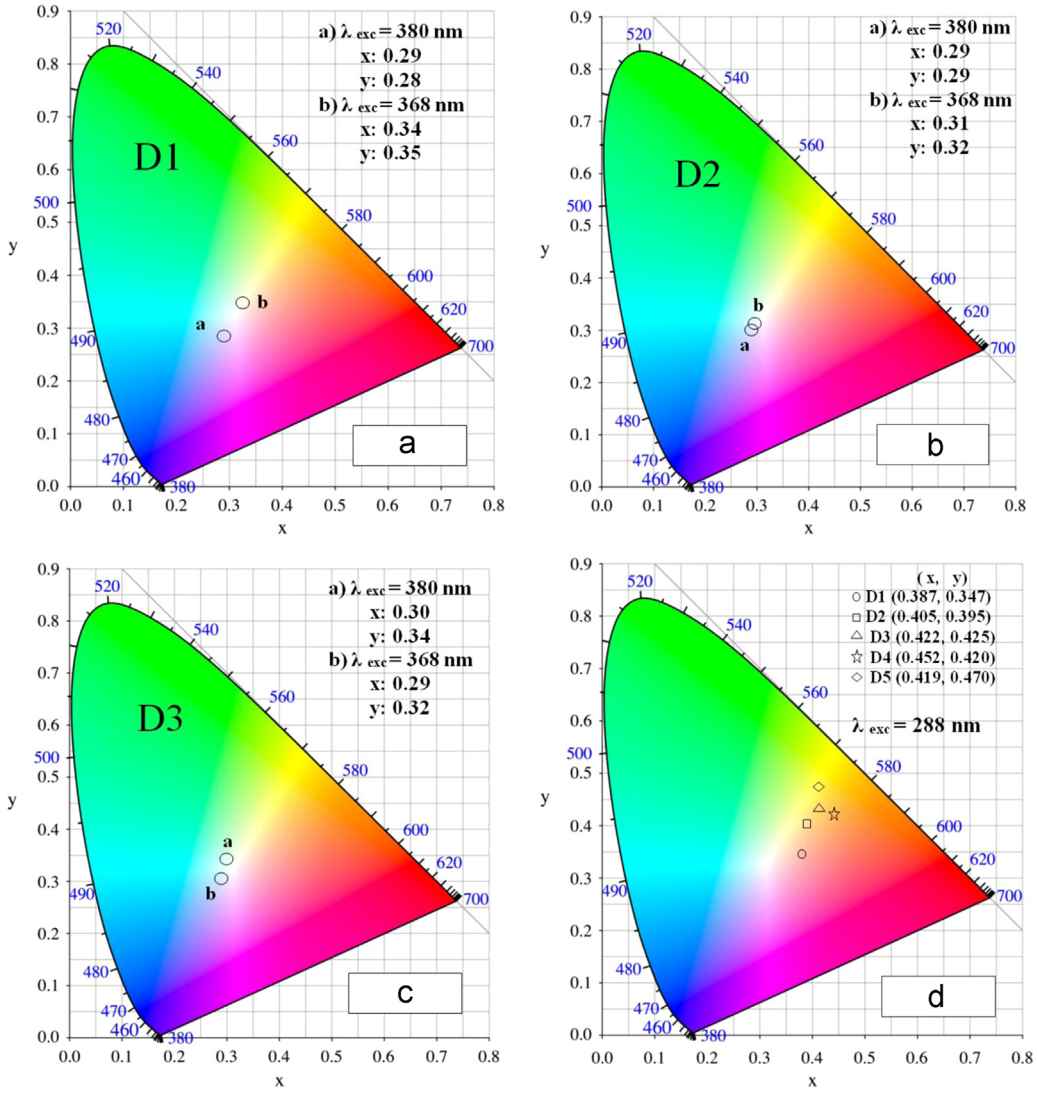

Fig. 10. CIE chromaticity diagrams for ZrO_2:Tb^{3+} + Eu^{3+} films deposited at 550 °C, excited with 368 and 380 nm (A, B and C) and excited with 288 nm (D) for different combinations (D1, D2, D3, D4, D5).

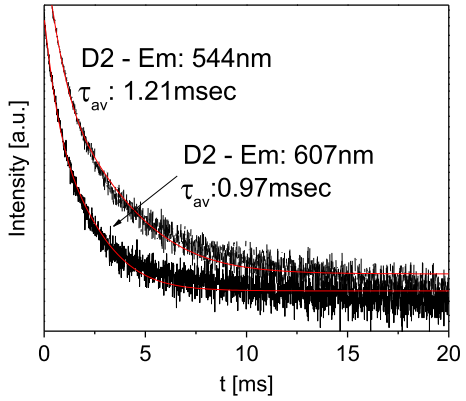

Fig. 11. Decay time for the sample D2 recorded for terbium emission at 544 nm and 607 nm for europium emission.

incorporated Zr was of approximately 25.98 at%. This value is relatively far from the ideal value of 33 at%, which may be due the incorporation of chlorine into the ZrO_2 host lattice. It is found that the multicolored emissions are strong enough to be easily viewed with the naked eye. The PL results from ZrO_2, Tb (or Eu)-doped and co-doped ZrO_2: Eu^{3+}+Tb^{3+} films showed multicolored emissions including colors such as blue (from host lattice), green (from ZrO_2: Tb^{3+} films), red-orange (from ZrO_2: Eu^{3+} films), yellow (from ZrO_2: Eu^{3+}+Tb^{3+} films excited with 288 nm) and bluish-white and yellowish-white (from ZrO_2: Eu^{3+}+Tb^{3+} films excited with 368 or 380 nm). Decay time measurements for the sample D2 showed average decay times of 1.21 and 0.97 ms. for Tb^{3+} and Eu^{3+} ions, respectively. The CIE coordinates of the double-doped ZrO_2: Tb^{3+} (10 at%)+Eu^{3+} (5 at%) films lie in the white light region of the chromaticity diagram and show promise as good phosphor materials for lighting devices and good candidates for use in photonic applications.

Acknowledgements

The authors wish to thank Adriana Tejeda for her support in carrying out the XRD study; J. Romero-Ibarra for SEM-EDS

measurements; Prof. Prashant Patil for the CIE program, also to A. Báez-Rodríguez, J.M. García-León, M. Guerrero and Z. Rivera for their technical support. Also we thank to SIP-IPN for the financial support through the project number 20140503. Finally, to CONACYT for the financial support given during this work.

References

[1] C.H. Kim, C.-H. II-E Kwon, Y.-J. Park, H.-S. Hwang, B.-Y. Bae, C.-H. Yu, G-Y Hong Pyun, Phosphors for plasma display panels, J. Alloys Comp. 311 (2000) 33–39.

[2] R.P. Rao, D.J. Devine, RE-activated lanthanide phosphate phosphors for PDP applications, J. Lumin. 87/89 (2000) 1260–1263.

[3] C.R. Ronda, Recent achievement in research on phosphors for lamps and displays, J. Lumin. 72/74 (1997) 49–54.

[4] L.S. Rohwer, A.M. Srivastava, Development phosphors for LED, Electrochem. Soc. Interface 12 (2003) 36–43.

[5] R.-J. Xie, N. Hirosaki, Silicon-based oxynitride and nitride phosphors for white LEDs, Rev. Sci. Technol Adv. Mater. 8 (2007) 7–8.

[6] S. Lange, I. Sildos, M. Hartmanova, J. Aarik, V. Kiisk, Luminescence properties of Sm^{3+}—doped polycrystalline ZrO_2, J. Non-Crystalline Solids 345 (2008) 4380–4382.

[7] F. Ramos-Brito, C. Alejo-Armenta, M. García-Hipólito, E. Camarillo, J. Hernández A, H. Murrieta S, C. Falcony, Photoluminescent emission of Pr^{3+} ions in different zirconia crystalline forms, Opt. Mater. 30 (2008) 1840–1847.

[8] L. Liu, Y. Wang, X. Zhang, K. Yang, Y. Bai, W. Chuanhai Huang, C. Han, Yinglin Song Li, Efficient two-color luminescence of Er^{3+}/Yb^{3+}/Li^{+}:ZrO_2 nanocrystals, Opt. Mater. 33 (2011) 1234–1238.

[9] Dimple P. Dutta Srirupa Mukherjee, N. Manoj, A.K. Tyagi, Sonochemically synthesized rare earth double-doped zirconia nanoparticles: probable candidate for white light emission, J. Nanopart. Res. 14 (2012) 814.

[10] YuanWang Lixin Liu, Yurong Su, Yizhu ZiweiMa, Haiting Xie, Changcheng Zhao, Zhenxing Chen, Erqing Xiew Zhang, Synthesis and white light emission of rare earth-doped HfO_2 nanotubes, J. Am. Ceram. Soc. 94 (2011) 2141–2145.

[11] G.A. Hirata, J. McKittrick, M. Avalos-Borja, J.M. Siqueiros, D. Devlin, Physical properties of Y_2O_3: Eu luminescent films grown by MOCVD and laser ablation, Appl. Surf. Sci., 113/114, , 1997, p. 509–514.

[12] S.B. Quadri, E.F. Skelton, P. Lubitz, N.V. Nguyen, H.R. Khan, Electron beam deposition of ZrO_2 & ZnO films, Thin Solid Films 290/291 (1996) 80–83.

[13] H. Tomaszewski, J. Haemers, N. De Roo, J. Denul, R. De Gryse, Yttria-stabilized zirconia thin films grown by r.f. magnetron sputtering from an oxide target, Thin Solid Films 293 (1997) 67–74.

[14] E. De la Rosa Cruz, L.A. Diaz Torres, P. Salas, V.M. Castaño, J. M. Hernández, Evidence of non-radiative energy transfer from the host to the active ions in monoclinic ZrO_2:Sm^{3+}, J. Phys. D: Appl. Phys. 34 (2001) L83–L86.

[15] M. Morita, M. Baba, H. Fujii, D. Rau, M. Yoshita, H. Akiyama, M. Herren., Photoluminescence properties and ultra-fast decay profiles of nanoparticles in sol–gel zirconia thin films $x$$ZrO_2$.100-$x$Cds:$Mn^{2+}$ and Eu^{3+}, J. Lumin. 94/95 (2001) 191–195.

[16] Y. Cong, B. Li, B. Lei, W. Li, Long lasting phosphorescent properties of Ti doped ZrO_2, J. Lumin. 126 (2007) 822–826.

[17] P. Peshev, I. Stamblova, S. Vassilev, P. Stefanov, V. Blaskov, K. Starbova, N. Starbov, Spray pyrolysis deposition of nanostructured zirconia thin films, Mater. Sci. Eng. B 97 (2003) 106–110.

[18] R. Reynoso-Manríques, J.A.I. Díaz-Góngora, J. Guzmán-Mendoza, T. Rivera-Montalvo, J.C. Guzmán-Olguín, P.V. Cerón-Ramírez, M. García-Hipólito, C. Falcony., Photo-, cathodo- and thermoluminescent properties of dysprosium-doped HfO_2 films deposited by ultrasonic spray pyrolysis, Appl. Radiat. Isotopes 92 (2014) 91–95.

[19] R.C. Garvie, The occurrence of metastable tetragonal zirconia as a crystallite size effect, J. Phys. Chem. 69 (1965) 1238–1246.

[20] K.H. Leong, Morphological control of particles generated from the evaporation of solution droplets: theoretical considerations, J. Aerosol. Sci. 18 (1987) 511–524.

[21] M. García-Hipólito, R. Martínez, O. Alvarez-Fregoso, E. Martínez, C. Falcony, Cathodoluminescent and photoluminescent properties of terbium doped ZrO_2 films prepared by pneumatic spray pyrolysis technique, J. Lumin. 93 (2001) 9–15.

[22] L. Jinsheng, Dan Zhou, Bin Yang, Ruiqing Liu, Qian Zhang, Sol–gel preparation and photoluminescence properties of tetragonal ZrO_2:Y^{3+}, Eu^{3+} nanophosphors, Opt. Mater. 35 (2012) 274–279.

[23] K. U., M. Part, T. Tätte, V. Kiisk, M.G. Brik, A.A. Chaykin, I. Sildos, Spectroscopic properties of Eu-doped Y-stabilized ZrO_2 microtubes, J. Lumin. 152 (2014) 125–128.